Neural Function in *DCC* Mutation Carriers with and without Mirror Movements

Daniel E. Vosberg, PhD,[1,2†] Vincent Beaulé, PhD,[3†] Angélica Torres-Berrío, PhD,[2,4] Danielle Cooke, BSc,[5] Amanda Chalupa, MSc,[1] Natalia Jaworska, PhD,[1,6] Sylvia M. L. Cox, PhD,[1] Kevin Larcher, MEng,[7] Yu Zhang, PhD,[7] Dominique Allard, BScN,[1] France Durand, MSc,[1] Alain Dagher, MD,[2,7] Chawki Benkelfat, MD, CSPQ, DERBH,[1,2,7] Myriam Srour, MD, PhD,[7] Donatella Tampieri, MD,[7] Roberta La Piana, MD,[7] Ridha Joober, MD, PhD,[1,2,4] Franco Lepore, PhD,[3] Guy Rouleau, MD, PhD,[7] Alvaro Pascual-Leone, MD, PhD,[5] Michael D. Fox, MD, PhD,[5] Cecilia Flores, PhD,[1,2,4] Marco Leyton, PhD,[1,2,7] and Hugo Théoret, PhD[3]

Objective: Recently identified mutations of the axon guidance molecule receptor gene, *DCC,* present an opportunity to investigate, in living human brain, mechanisms affecting neural connectivity and the basis of mirror movements, involuntary contralateral responses that mirror voluntary unilateral actions. We hypothesized that haploinsufficient $DCC^{+/-}$ mutation carriers with mirror movements would exhibit decreased *DCC* mRNA expression, a functional ipsilateral corticospinal tract, greater "mirroring" motor representations, and reduced interhemispheric inhibition. $DCC^{+/-}$ mutation carriers without mirror movements might exhibit some of these features.

Methods: The participants (n = 52) included 13 $DCC^{+/-}$ mutation carriers with mirror movements, 7 $DCC^{+/-}$ mutation carriers without mirror movements, 13 relatives without the mutation or mirror movements, and 19 unrelated healthy volunteers. The multimodal approach comprised quantitative real time polymerase chain reaction, transcranial magnetic stimulation (TMS), functional magnetic resonance imaging (fMRI) under resting and task conditions, and measures of white matter integrity.

Results: Mirror movements were associated with reduced *DCC* mRNA expression, increased ipsilateral TMS-induced motor evoked potentials, increased fMRI responses in the mirroring M1 and cerebellum, and markedly reduced interhemispheric inhibition. The $DCC^{+/-}$ mutation, irrespective of mirror movements, was associated with reduced functional connectivity and white matter integrity.

Interpretation: Diverse connectivity abnormalities were identified in mutation carriers with and without mirror movements, but corticospinal effects and decreased peripheral *DCC* mRNA appeared driven by the mirror movement phenotype.

ANN NEUROL 2019;85:433–442

The axon guidance molecule receptor, DCC (deleted in colorectal cancer), plays a critical role in directing normal decussation of corticospinal tract (CST) and commissural pathways. In homozygous *DCC* mutant mice, the ensuing failure of axonal interhemispheric crossing is associated with a lack of asymmetric movements.[1] Similar to the murine

View this article online at wileyonlinelibrary.com. DOI: 10.1002/ana.25418

Received Feb 14, 2018, and in revised form Jan 18, 2019. Accepted for publication Jan 18, 2019.

Address correspondence to Dr Leyton, McGill University, Irving Ludmer Building, Montreal, QC, Canada, H3A 1A1; Email: marco.leyton@mcgill.ca and Dr Théoret, Université de Montréal, Pavillon Marie-Victorin, Montreal, QC, Canada, H2V 2S9; Email: hugo.theoret@umontreal.ca

Current address for Dr Torres-Berrío: Fishberg Department of Neuroscience and Friedman Brain Institute, Icahn School of Medicine at Mount Sinai, New York, NY.

†D.E.V. and V.B. share first coauthorship.

From the [1]Department of Psychiatry, McGill University, Montreal, Quebec, Canada; [2]Integrated Program in Neuroscience, McGill University, Montreal, Quebec, Canada; [3]Department of Psychology, University of Montreal, Montreal, Quebec, Canada; [4]Douglas Mental Health University Institute, Montreal, Quebec, Canada; [5]Beth Israel Deaconess Medical Center, Harvard Medical School, Boston, MA; [6]Institute of Mental Health Research, affiliated with the University of Ottawa, Ottawa, Ontario, Canada; and [7]Neurology and Neurosurgery, McGill University, Montreal, Quebec, Canada

motor phenotype, humans with *DCC* mutations exhibit mirror movements (MM); that is, voluntary actions on one side of the body elicit simultaneous involuntary movements on the contralateral side.[2]

The human *DCC* mutation–related MM are substantially more pronounced than the smaller MM that are commonly exhibited by young children and then, at around age 10 years, disappear following maturation of the corpus callosum (CC) and the development of normal interhemispheric inhibition (IHI).[3] Also unlike healthy children, adults with severe congenital MM exhibit evidence of a pronounced ipsilateral CST,[4–8] and among the recently identified *DCC* mutation carriers, some have agenesis of the CC, MM, both phenotypes, or neither phenotype.[8–10]

A number of important features in *DCC* mutation carriers remain unknown. It is unknown whether they exhibit abnormal motor cortex activations, motor system connectivity, or interhemispheric function. The neurophysiological phenotype of *DCC* mutation carriers without MM is unknown. There is currently no explanation to account for the partial penetrance of MM among mutation carriers.

To map in detail the neurocircuitry of *DCC* mutation–related MM, we have completed multimodal neuroimaging in 33 members of a large, 4-generational Quebec family with a *DCC* frameshift mutation (NM_005215.3, c.1140 + 1G > A). This mutation results from abnormal skipping of exon 6, leading to a premature stop codon that encodes a truncated DCC protein that fails to bind to its ligand, netrin.[2] Our a priori predictions were that, relative to controls, *DCC* mutation carriers with MM would exhibit an increased functional ipsilateral CST, increased "mirroring" motor representations, reduced IHI, alterations in motor and interhemispheric anatomical and functional connectivity, and decreased *DCC* mRNA expression. Finally, we sought to determine the effects of the *DCC* mutation, potentially distinct from the effects of MM.

Subjects and Methods

Participants

Fifty-two volunteers participated in the study (Table 1, Fig 1). This included 13 *DCC* haploinsufficient individuals with MM ($DCC^{+/-}$/MM^{+}), 7 *DCC* haploinsufficient individuals without MM ($DCC^{+/-}$/MM^{-}), and 13 relatives with neither the mutation nor MM ($DCC^{+/+}$/MM^{-}); 19 unrelated healthy volunteers (UHVs) were tested to control for *DCC* familial features unrelated to the mutation. Participant safety screening procedures were completed prior to magnetic resonance imaging (MRI) and transcranial magnetic stimulation (TMS). All participants gave written informed consent, and the protocol was carried out in accordance with the Declaration of Helsinki and approved by the relevant research ethics committees.

Genetics

Participants who had not been genotyped previously[2] were characterized for *DCC* variants. Genotyping was unavailable for 1 UHV, who only completed the MRI, and excluding this individual did not alter the findings. Coding exons and the exon–intron boundaries of *DCC* were screened for mutations based on sequence (NM_005215; UCSC March 2006 Assembly HG 18). Primers were the same as used previously.[2] Polymerase chain reaction (PCR) products were sequenced on the ABI 3700 sequencer at the Genome Quebec Centre for Innovation according to the manufacturer's recommended protocol (Applied Biosystems, Foster City, CA). Sequences were aligned and analyzed using SeqMan 4.03 (DNASTAR, Madison, WI) and Mutation Surveyor v3.1 (SoftGenetics, State College, PA).

Mirror Movements

Prior to testing, 2 self-adhesive electrodes were placed on the first dorsal interosseous (FDI) muscle bilaterally and a ground electrode was positioned on the right wrist. The electromyographic (EMG) signal was amplified using a Powerlab 4/30 system (ADInstruments, Colorado Springs, CO), filtered with a bandpass of 20 to 1,000 Hz, and digitized at a sampling rate of 4 kHz. First, seated participants were asked to relax their arms with their palms facing upward, supported by their legs. They were instructed to respond to an auditory signal by pressing, then releasing, a small stress ball 3 times with one hand while the other hand was at rest. This protocol was performed for both hands and repeated 5 times. To assess subtler MM, a protocol known to generate physiological MM (pMM) in healthy participants was performed.[3] Participants were instructed to maintain a tonic contraction with one hand (using the minimal strength needed to hold a pencil without dropping it). Meanwhile, participants were required to respond to an auditory signal with their other hand by performing a voluntary phasic pinch contraction. This was performed 20 times for both hands. pMM were defined as a significant increase in the background EMG activity of the hand maintaining the tonic contraction, starting at the moment of the phasic contraction and lasting 100 milliseconds, compared to 1,000 milliseconds of background activity prior to the phasic contraction. Data were expressed as the ratio of EMG activity in the tonically contracting hand during phasic contraction of the contralateral hand over background activity preceding phasic contraction. The data from both hemispheres were averaged.

Single-Pulse TMS

TMS was delivered through an 8 cm figure-of-eight coil connected to a Magstim 200 stimulator (Magstim, Whitland, UK) with a monophasic current waveform in a posterior–anterior orientation. The coil was positioned flat on the scalp at an angle of 45° from the midline. Single-pulse stimulation was performed over the hand area of primary motor cortex (M1) at the optimal position (hot spot) eliciting motor evoked potentials (MEPs) of maximal amplitude in the contralateral FDI muscle. The hot spot was marked on the scalp with a pen to ensure stable coil positioning throughout the experiment. Stimulation intensity was adjusted to elicit contralateral MEPs of 1 mV amplitude. MEPs were recorded using Scope

TABLE 1. Participant Characteristics

Characteristic	Group				
	$DCC^{+/-}$/MM^{+}	$DCC^{+/-}$/MM^{-}	$DCC^{+/+}$/MM^{-}	UHV	Statistical Test, 4 Groups
N_{total}	13	7	13	19	
N_{MRI}	11	7	12	19	
$N_{task\text{-}fMRI}$	11	7	12	18	
$N_{rs\text{-}fcMRI}$	10	7	12	14	
N_{TMS}	12	7	12	14	
Age, mean ± SD	44.4 ± 16.9	49.6 ± 14.9	37.9 ± 13.2	41.4 ± 16.3	$F_{3, 48} = 0.96$, $p = 0.42$
Sex, M:F	9:4	2:5	5:8	10:9	$\chi^2_3 = 3.95$, $p = 0.27$
Handedness	11 right, 2 left	5 right, 2 left	10 right, 3 left	19 right	$\chi^2_3 = 5.40$, $p = 0.15$

$DCC^{+/-}$/MM^{-} mutation carriers without MM; $DCC^{+/-}$/MM^{+} = mutation carriers with MM; $DCC^{+/+}$/MM^{-} = relatives without the mutation or MM; F = female; M = male; MRI = magnetic resonance imaging; rs-fcMRI = resting state functional connectivity MRI; SD = standard deviation; TMS = transcranial magnetic stimulation; UHV = unrelated healthy volunteers; MM = mirror movements.

v4.0 software (ADInstruments). The EMG signal was filtered with a bandwidth of 20 to 1,000 Hz and digitized at a sampling rate of 4 kHz. Single-pulse stimulation was performed over the hand area of M1 while participants were at rest with eyes open, 10 times for each hemisphere, and MEPs were recorded bilaterally in the FDI muscle to confirm the presence or absence of mirror MEPs in all participants. Peak-to-peak amplitudes of contralateral and ipsilateral MEPs were measured and averaged offline. Relative amplitudes of ipsilateral and contralateral MEPs were expressed as an ipsilateral coefficient (ipsilateral MEP amplitude/contralateral MEP amplitude). MEP traces were monitored online to ensure that no muscle activity in the 100-millisecond window prior to TMS was present. Trials with prestimulus activity were discarded and repeated, and were < 1% of all trials. The data from both hemispheres were averaged. Contralateral and ipsilateral TMS-induced MEP latencies were also measured, from TMS pulse to MEP onset.

Double-Coil TMS

IHI was measured using a protocol described by Ferbert and collaborators using two 50 mm custom-made coils connected to 2 Magstim 200 stimulators.[11] Each coil was placed over its respective M1 hot spot over the right and left hemispheres. The intensity of each TMS pulse was adjusted to elicit MEPs of approximately 1 mV contralaterally. A test stimulus was preceded by a conditioning stimulus applied 40 milliseconds earlier. IHI was measured for left-to-right and right-to-left directions of inhibition. IHI was expressed as the ratio of double stimulation MEPs over single-pulse MEPs. The data for both directions were averaged.

MRI Parameters

Participants underwent anatomical, diffusion-weighted, resting-state functional, and 2 identical task functional MRI (fMRI) acquisitions in a scanning session using a 3 T Siemens (Erlangen, Germany) Magnetom Trio MRI scanner (32 channel head coil). The high-resolution, T1-weighted anatomical acquisition parameters were as follows: inversion time/repetition time (TR)/echo time (TE) = 900/2,300/2.98 milliseconds, flip angle = 9°, slice thickness = 1.0 mm (1 mm isotropic voxel size), with a field of view (FOV) of 256 × 256 mm^2 and duration of 9 minutes 50 seconds. Participants underwent diffusion tensor imaging (DTI) using a single-shot spin-echo echo-planar pulse sequence with multidirectional diffusion weighting (TR/TE = 12,000/89 milliseconds, 90 contiguous axial slices with an isotropic 2 mm resolution, FOV = 256 × 256 mm^2, matrix size = 128 × 128 with partial Fourier reconstructed to 6/8). Diffusion weighting was distributed evenly on the unit hemisphere using 64 noncollinear gradients and a b value of 1,000. One additional volume with no diffusion weighting (ie, b value = 0) was acquired in the beginning

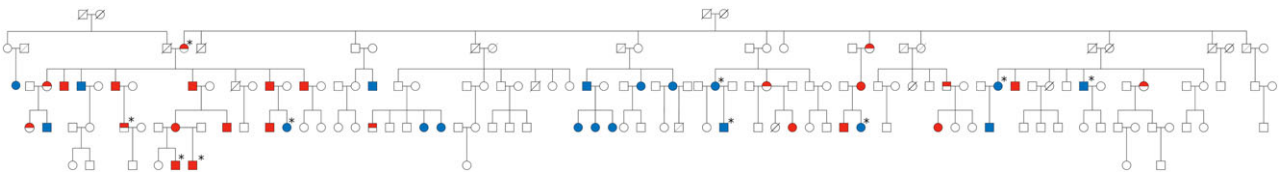

FIGURE 1: Pedigree of Quebec family. Full red indicates $DCC^{+/-}$/MM^{+}; half red indicates $DCC^{+/-}$/MM^{-}, blue indicates $DCC^{+/+}$/MM^{-} relatives, white designates those who did not undergo genetic testing. Asterisks (*) indicate previously genotyped individuals who did not participate in the present study. Crossed lines designate deceased. Squares and circles are males and females, respectively. [Color figure can be viewed at www.annalsofneurology.org]

of the acquisition. The task fMRI acquisition parameters were as follows: TR/TE = 1,500/30 milliseconds, flip angle = 90°, slice thickness = 4.0 mm (4 mm isotropic voxel size), slices = 28, FOV = 256 × 256 mm^2, and duration of 6 minutes 8 seconds. The resting state fMRI acquisition parameters were as follows: TR/TE = 2,000/30 milliseconds, flip angle = 90°, slice thickness = 4.0 mm (4 mm isotropic voxel size), slices = 38, FOV = 256 × 256 mm^2, and duration of 6 minutes 8 seconds.

Resting State Functional Connectivity MRI

Resting state functional connectivity MRI (rs-fcMRI) data were processed as described previously,[12,13] including slice-acquisition–dependent time shifts, head motion correction, atlas registration, spatial smoothing (6 mm full width at half maximum [FWHM]), low-pass temporal filtering ($f < 0.08$ Hz), and removal of confounding variables by linear regression including head motion, the whole-brain (global) signal, and signals from the ventricles and white matter (WM). A metric of overall movement was also computed for use as a covariate by computing the root mean square of the rotation, translation, and displacement of the brain relative to the time point before it, then averaging across all time points.[14] A priori regions of interest (ROIs; 6 mm radius spheres) were generated in the left and right M1 (Montreal Neurological Institute [MNI] coordinates: −41, −20, 62 and 41, −20, 62) based on a prior fMRI study of hand movements.[15] A priori ROIs were also generated in the left and right cerebellum (MNI coordinates: −20, −52, −24 and 17, −52, −24) based on prior functional connectivity with left and right M1.[15] rs-fcMRI between motor ROIs (1 comparison), between motor and cerebellar ROIs (4 comparisons), and between motor ROIs and all other brain voxels were computed.[12] For statistical comparisons, correlation coefficients (r values) from each subject were converted to a normal distribution using Fisher r to z transform. For the fMRI 2nd level analyses, a full factorial using the same design described below in the Statistical Analyses section with the addition of total movement during the MRI as a covariate was run in SPM12. Because generalized estimating equations (GEEs) are not possible with Statistical Parametric Mapping (SPM), family was instead entered as a fixed factor.

Task fMRI

fMRI analyses were conducted using SPM 12 software (Wellcome Department of Imaging Neuroscience, University College London, London, UK). fMRI images were slice-time corrected, realigned, coregistered to the T1 image, segmented, normalized to standardized MNI space, and spatially smoothed with an 8 mm FWHM Gaussian kernel. For each participant, a general linear model was generated in SPM per task, consisting of the following conditions: (1) motor activity and rest and (2) somatosensory stimulation and rest, which were convolved with the hemodynamic response function. For group analyses, single-subject contrast images were entered into a random effect model. Block design motor and somatosensory fMRI tasks comprised 18 seconds of activity (motor: opening and closing right index finger and thumb; somatosensory: tactile stimulation on distal phalanx of right index finger) followed by 18 seconds of rest, for a total of 10 blocks per condition. The somatosensory stimulation was conducted using circular domes (25 mm diameter), fabricated from solid plastic with deep rectangular grooves cut into the surface (3 mm equidistant grooves and bars; JVP Domes; Stoelting Co, Wood Dale, IL). The left arm, hand, and fingers were restrained throughout. For the motor task, as with the rs-fcMRI analysis, a priori ROIs (6 mm radius spheres) were generated in the left and right M1 (MNI coordinates: −41, −20, 62 and 41, −20, 62) as well as the left and right cerebellum (MNI coordinates: −20, −52, −24 and 17, −52, −24). For the somatosensory task, a priori ROIs (6 mm radius spheres) were generated in the left and right somatosensory cortex (MNI coordinates: −42, −35, 65 and 42, −35, 65). Additionally, a single-blind investigator manually segmented the hand knob region of M1 using the McConnell Brain Imaging Centre MINC tool, Display.[16] Following quality control, verifying the coregistration of each participant's T1 image, "default" left hand knob ROI, and right hand–induced motor task functional activation, 2 participants were excluded. Finally, mean beta weights were extracted from ROIs using MarsBar 0.44. As for the rs-fcMRI data, a full factorial using the same design described below in the Statistical Analyses section was run in SPM12 for the fMRI 2nd-level analyses, and family was entered as a fixed factor, because GEEs are not possible with SPM.

Diffusion-Weighted Imaging of CC

Images were denoised using NLMEANS denoising[17] as implemented in Dipy.[18] Magnetic field inhomogeneities were corrected using the N4 correction from ANTS.[19] A brain mask was extracted using BET from the FSL toolkit,[20,21] which was used in conjunction with the FSL Eddy tool to correct for motion, eddy currents, and susceptibility artifacts.[20,22] The T1 images were also denoised using NLMEANS, field inhomogeneities were corrected (N4 correction), and a brain mask was extracted (BET). The diffusion-weighted imaging (DWI) datasets were then upsampled to 1 × 1 × 1 resolution, and tensor-based diffusion metrics were computed using Dipy. Fiber orientation distribution functions were estimated using a fixed response function, set to correspond to a pure myelinated axon response (15, 4, 4×10^{-4} mm^2/s). The T1 image was registered to the upsampled DWI using ANTS. A WM mask was segmented from the registered T1 using ANTS and was used for deterministic and probabilistic local tracking (as defined by Descoteaux et al[23]), which was run using 5 seeds per voxel of the WM mask, only keeping streamlines reaching the gray matter. Step size was 0.5 mm. Following generation of the whole-brain tractogram, bundles composing the CC were automatically extracted using a modified version of the RecoBundles algorithm. In this algorithm, the whole-brain tractogram was first registered to the atlas,[24] and bundles were individually extracted based on centroids and distances to the atlas.[25] The atlas comprises 20 major WM bundles, presegmented on 4 different healthy subjects from the Human Connectome Project dataset. Those segmentations were validated by 2 neuroanatomists for consistency with generally accepted anatomical definitions, and were used as references for the segmentation process. Subparts of the CC were segmented from the reference subject into 7 subparts as previously

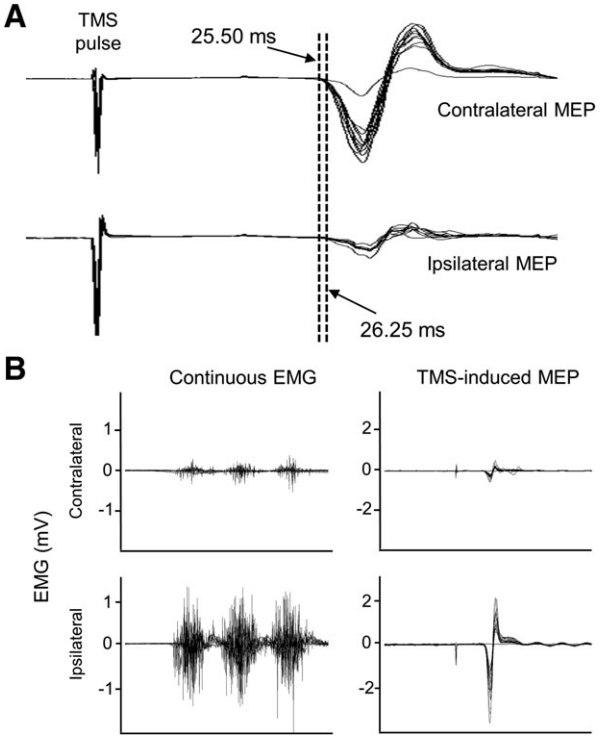

FIGURE 2: Transcranial magnetic stimulation (TMS)/electromyography (EMG). (A) Raw EMG traces of TMS-induced motor evoked potentials (MEPs) in a *DCC*$^{+/-}$/mirror movements (MM)$^{+}$ individual with larger MEPs in the hand contralateral to stimulation. Dashed lines indicate the onset of TMS-induced MEPs. (B) Raw EMG traces of TMS-induced MEPs and continuous EMG in a *DCC*$^{+/-}$/MM^{+} individual with larger MEPs in the hand ipsilateral to stimulation.

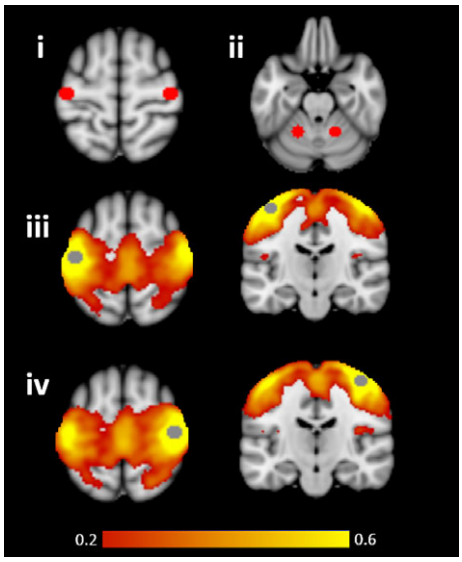

FIGURE 3: Resting state functional connectivity magnetic resonance imaging. A priori regions of interest are shown in the left and right primary motor cortex (i) and the left and right cerebellum (ii). Functional connectivity with the left primary motor cortex (iii) and right primary motor cortex (iv) is shown averaged across all participants. [Color figure can be viewed at www.annalsofneurology.org]

defined.[26] Fractional anisotropy (FA), mean diffusivity (MD), radial diffusivity (RD), and axial diffusivity (AD) values were extracted for each CC segment.

Lymphoblastoid Cell Line Growth, RNA Extraction, and Quantitative Real Time PCR

DCC mRNA expression was measured by performing RNA extraction followed by quantitative real time PCR, as previously described,[27] using lymphoblastoid cell lines (LCLs) extracted from blood collected from the participants. LCLs established by transformation with Epstein–Barr virus were grown using standard protocols.[28] Total RNA was isolated from the lymphoblastoid cell lines with the miRNeasy Micro Kit protocol (Qiagen, Toronto, Ontario, Canada). All RNA samples were determined to have 260/280 and 260/230 values ≥1.8, using the Nanodrop 1000 system (Thermo Fisher Scientific, Toronto, Ontario, Canada). Reverse transcription for *DCC* mRNA (2 mg) was performed using the High-Capacity cDNA Reverse Transcription Kit (Applied Biosystems, Toronto, Ontario, Canada). Real time PCR using TaqMan probes (Thermo Fisher Scientific) was carried out with an Applied Biosystems QuantStudio 6-Flex Real Time PCR system. Data for *DCC* mRNA expression were analyzed by using the absolute quantitation standard curve method. Real time PCR was run in technical triplicates. The LCL sample (n = 37) included 10 *DCC*$^{+/-}$/MM^{+}, 6 *DCC*$^{+/-}$/MM^{-}, 11 *DCC*$^{+/+}$/MM^{-}, and 10 UHVs. This included 4 previously genotyped individuals (2 *DCC*$^{+/-}$/MM^{-} and 2 *DCC*$^{+/+}$/MM^{-}) who did not participate in the present neuroimaging study. Four outliers were removed, as identified by GraphPad (La Jolla, CA) Prism 7's ROUT test for definitive outliers (Q = 0.1%).

Statistical Analyses

Using SPSS20, ipsilateral EMG data, physiological MM, ipsilateral/contralateral MEP coefficients, IHI, fiber integrity of the CC, fMRI motor responses, and *DCC* mRNA expression were each analyzed using GEEs, with an exchangeable working correlation matrix. These analyses coded for the 2 fixed factors of (1) the presence of MM and (2) the presence of the *DCC* mutation. To control for the correlations among family members, driven by shared genetics and environments, we defined clusters by the branches within the Quebec family, descending from the earliest generation. Moreover, each unrelated healthy volunteer comprised their own cluster. Additionally, age was used as a covariate due to previously reported age-related effects of DCC[29–31] and of the motor system, as assessed with MRI and TMS.[32–34] For the EMG, ipsilateral/contralateral MEP coefficients, and physiological MM analyses, the data did not satisfy assumptions of normality and consequently were log-transformed. Log transformations were not appropriate for the task fMRI or *DCC* mRNA data, due to negative values and the transformations rendering the data less Gaussian. However, sensitivity analyses and inspection of the residuals revealed that these data were approximately normal. The MD, RD, and AD of the CC values were highly non-normal, as indicated by normality tests and plots, and were unimproved by log transformations. Therefore, these data were not appropriate for GEE analyses and no

TABLE 2. Pairwise Connectivity Values

Group	Right M1 to Left Cerebellum	Right M1 to Right Cerebellum	Right M1 to Left M1	Left M1 to Left Cerebellum	Left M1 to Right Cerebellum
$DCC^{+/-}/MM^{+}$	0.098	−0.110	0.707	0.075	0.062
$DCC^{+/-}/MM^{-}$	−0.087	−0.208	0.514	−0.037	−0.030
$DCC^{+/+}/MM^{-}$	0.173	−0.102	0.759	0.061	0.019
UHV	0.014	−0.052	0.818	−0.124	0.024

Average Fisher *Z* score values between a priori regions of interest for $DCC^{+/-}/MM^{+}$, $DCC^{+/-}/MM^{-}$, $DCC^{+/+}/MM^{-}$, and UHV.
M1 = primary motor cortex; MM = mirror movements; UHV = unrelated healthy volunteer.

significant effects were detected following sensitivity analyses, comprising the removal of the most extreme outliers, identified using Prism 7's ROUT test for definitive outliers (Q = 0.1%).

Results

TMS and Electromyography

GEE analyses revealed that increased EMG activity in the mirroring hand during voluntary unilateral contractions was associated with the presence of MM (β = 0.829, 95% confidence interval [CI] = 0.457–1.201, p = 0.000013) but not with the *DCC* mutation (β = 0.156, 95% CI = −0.134 to 0.446, p = 0.293). Similarly, increases in the ratio of ipsilateral/contralateral MEPs induced by unilateral single-pulse TMS of the M1 hand area were associated with MM (β = 1.666, 95% CI = 1.498–1.833, p < 0.00001) but, again, not the *DCC* mutation (β = −0.024, 95% CI = −0.290 to 0.243, p = 0.862).

The ipsilateral MEPs detected among the $DCC^{+/-}/MM^{+}$ participants occurred in 100% of trials. There was no effect of MM on the size of contralateral MEPs ($F_{1,\ 40}$ = 0.0001, p = 0.99). Among the $DCC^{+/-}/MM^{+}$ participants, the amplitudes of ipsilateral MEPs, relative to contralateral MEPs, were smaller in 7 participants and larger in 5. Three participants presented ipsilateral MEPs that were > 5 times larger than their contralateral counterparts. Ipsilateral (mean [M] = 23.80, standard deviation [SD] = 3.05) and contralateral (M = 23.50, SD = 2.79) MEP latencies were nearly identical in the $DCC^{+/-}/MM^{+}$ group and not

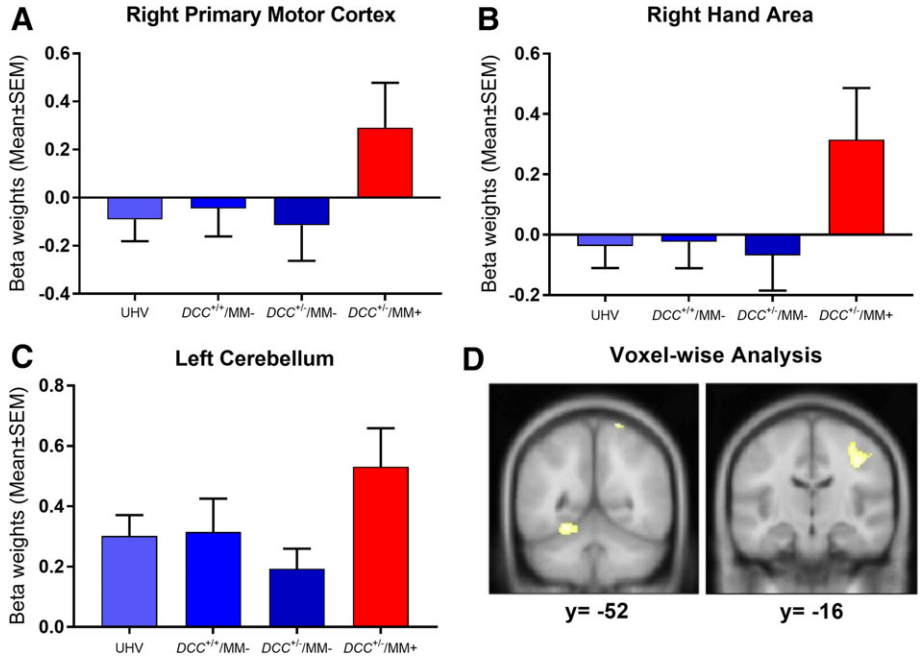

FIGURE 4: Task functional magnetic resonance imaging. (A–C) Increased right-hand–induced activations associated with the presence of mirror movements in the ipsilateral (A) right primary motor cortex (M1) and (B) right M1 hand area, and in the contralateral (C) left cerebellum. (D) Peak activation sites in whole-brain voxelwise analysis (p < 0.001) in left cerebellum and right M1. Raw data are plotted. MM = mirror movements; SEM = standard error of the mean; UHV = unrelated healthy volunteers. [Color figure can be viewed at www.annalsofneurology.org]

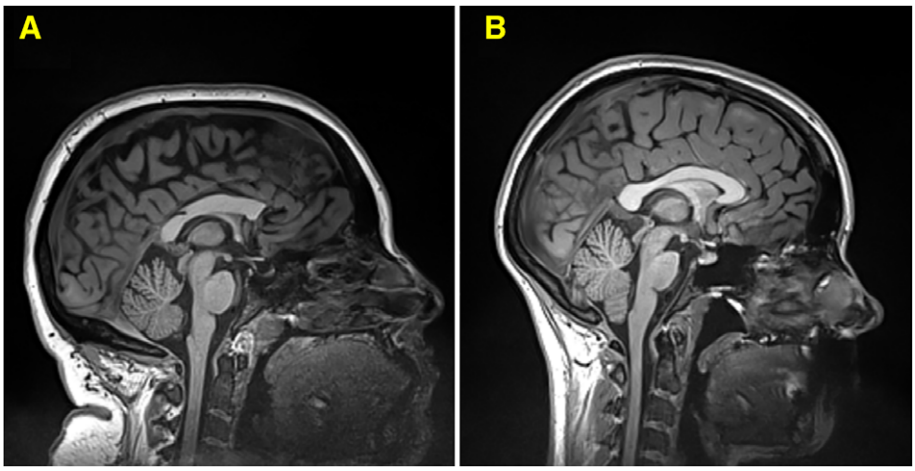

FIGURE 5: Partial agenesis of the corpus callosum. (A) Partial agenesis of the corpus callosum in female individual with a *DCC* mutation and without mirror movements, revealing absence of the rostrum. (B) Female unrelated healthy volunteer without a *DCC* mutation or mirror movements, for comparison. [Color figure can be viewed at www.annalsofneurology.org]

significantly different ($F_{1,11}$ = 2.2, p = 0.16), suggesting that the ipsilateral MEPs resulted from fast-conducting, ipsilateral CST projections (Fig 2).

Increased pMM were associated with MM (β = 0.437, 95% CI = 0.402–0.472, p < 0.00001). Again, these effects were uniquely associated with MM, as there were no significant effects of the *DCC* mutation on pMM (β = −0.007, 95% CI = −0.044 to 0.031, p = 0.735). Finally, reductions in IHI, indicated by increased responses following double-coil TMS, were associated with MM (β = 0.531, 95% CI = 0.337–0.724, p < 0.00001). There were no significant effects of the *DCC* mutation on IHI (β = −0.028, 95% CI = −0.291 to 0.235, p = 0.833).

Resting State and Task fMRI

Functional connectivity was evaluated between our a priori ROIs (Fig 3). Between the right M1 and left M1, reduced functional connectivity was associated with the *DCC* mutation (β = −0.259, 95% CI = −0.517 to 0.000, p = 0.0497). Moreover, between the right M1 and left cerebellum, decreased connectivity was associated with the *DCC* mutation (β = −0.245, 95% CI = −0.436 to −0.054, p = 0.012) and increased connectivity was associated with MM (β = 0.245, 95% CI = 0.062–0.428, p = 0.009). See Table 2 for all pairwise connectivity values. A whole-brain voxelwise search found no significant abnormalities (after familywise error [FWE] correction) in right M1 or left M1 connectivity.

Consistent with the reduction in IHI, increases in mirroring fMRI motor responses were associated with the presence of MM. Right hand–induced, right sphere–based M1 activations were associated with MM (β = 0.498, 95% CI = 0.073–0.922, p = 0.0215) and not the *DCC* mutation (β = −0.174, 95% CI = −0.446 to 0.099, p = 0.211; Fig 4). Similarly, in the right manually segmented hand area, increased right hand–induced activations were associated with MM (β = 0.462, 95% CI = 0.101–0.822, p = 0.012) and not with the *DCC* mutation (β = −0.138, 95% CI = −0.356 to 0.079, p = 0.212). Moreover, in the left cerebellum, increased right hand–induced activations were associated with MM (β = 0.398, 95% CI = 0.107–0.689, p = 0.007), whereas decreased activations were associated with the *DCC* mutation (β = −0.185, 95% CI = −0.366 to −0.004, p = 0.045). Small volume–corrected voxelwise analysis revealed a similar pattern of effects, whereby increased activation was associated with the presence of MM in the right M1 (t = 3.36, p_{FWE} = 0.009) and left cerebellum (t = 3.62, p_{FWE} = 0.005). Although these findings did not survive a whole-brain correction, the peak activation sites and largest clusters across the whole brain (p < 0.001) were

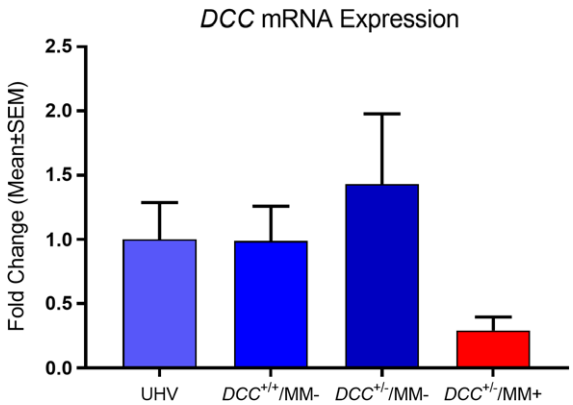

FIGURE 6: *DCC* mRNA. Decreased *DCC* mRNA (quantity mean: *DCC*/glyceraldehyde-3-phosphate dehydrogenase) fold change, originating from both the functioning and mutated allele, is associated with the presence of mirror movements and not the *DCC* mutation. Raw data are plotted. MM = mirror movements; SEM = standard error of the mean; UHV = unrelated healthy volunteers. [Color figure can be viewed at www.annalsofneurology.org]

in the right motor cortex (t = 4.21, MNI coordinates: 38, −16, 40) and left cerebellum (t = 4.07, MNI coordinates: −26, −52, −16). As exploratory analyses, there were no significant effects identified in the analyses of the default left M1, left hand area, or right cerebellum (all $p \geq 0.20$) or for the somatosensory task (all $p \geq 0.07$).

DTI and CC

Subtle reductions in FA were associated with the *DCC* mutation in the anterior midbody (β = −0.023, 95% CI = −0.042 to −0.003, p = 0.022), posterior midbody (β = −0.021, 95% CI = −0.036 to −0.005, p = 0.0078), isthmus (β = −0.017, 95% CI = −0.033 to 0.000, p = 0.048), and splenium (β = −0.016, 95% CI = −0.029 to −0.002, p = 0.021). Following sensitivity analyses of non-normally distributed AD, MD, and RD data, no significant effects were identified in these measures. Partial agenesis of the CC with an absent rostrum was observed in 1 female $DCC^{+/-}$/MM^{-} participant, as evaluated by a board-certified neuroradiologist (Fig 5).

DCC mRNA Expression

Quantitative real time PCR using RNA extracted from LCLs identified a significant reduction in *DCC* mRNA expression associated with the presence of MM (β = −1.056, 95% CI = −1.660 to −0.451, p = 0.00062). There was no significant effect of the *DCC* mutation alone (β = 0.265, 95% CI = −0.164 to 0.694, p = 0.226; Fig 6).

Discussion

The present study demonstrates that $DCC^{+/-}$/MM^{+} participants exhibit diverse functional and anatomical connectivity alterations, including increased mirroring activations in motor regions and reduced IHI. Ipsilateral CSTs among the $DCC^{+/-}$/MM^{+} individuals are strongly suggested by the similar latencies between TMS-induced ipsilateral and contralateral MEPs. Strikingly, for the first time, we show distinct alterations of the motor system among $DCC^{+/-}$ mutation carriers, independently of MM. We also provide a possible mechanism underlying the partial penetrance of MM, as a reduction in peripheral *DCC* mRNA expression was only associated with the presence of MM and not the *DCC* mutation.

Contrary to what has been observed in $RAD51^{+/-}$/MM^{+} individuals,[7] where mirror MEPs were elicited in no more than one-third of TMS trials using 1.2x resting motor threshold intensity, mirror MEPs were induced in 100% of trials among $DCC^{+/-}$/MM^{+} participants using a similar stimulation intensity at rest (1 mV MEP),[35] consistent with recent reports.[10] Therefore, it appears that downregulating DCC, compared to RAD51, has a larger impact on the development and excitability of the ipsilateral CST. Whereas DCC's role in guiding commissural and corticospinal axons has been characterized in vitro and in vivo,[1,10,36,37] RAD51 is less well understood but is expressed at the pyramidal decussation.[38] Further elucidation of the molecular mechanisms is needed to explain phenotypic differences in CST between *DCC* and *RAD51* mutation carriers.

Previous studies have indicated greater mirroring motor representations among individuals with MM,[6,7,39] but our study restrained the mirroring arm, hand, and fingers, minimizing the possibility that the motor activation is simply an artifact of the movement in the mirroring hand. Instead, it appears that the reduced IHI results in increased mirroring motor representations. Our findings strongly suggest that unilateral motor control of the hand relies on selective corticospinal wiring between the motor cortex and contralateral hand, as well as on normal interhemispheric communication.

A previous report indicated that some *DCC* and *RAD51* mutation carriers without visually apparent MM nonetheless exhibited subtle MM.[40] In comparison, we did not detect any evidence of increased pMM in $DCC^{+/-}$/MM^{-} individuals. However, we did identify evidence of reduced functional connectivity and WM integrity associated with the $DCC^{+/-}$ mutation (independent of mirror movements), suggesting a neurophysiologically altered motor system in individuals with an abnormal *DCC* gene.

Although only some $DCC^{+/-}$ carriers exhibit MM, both MM^{+} and MM^{-} $DCC^{+/-}$ groups exhibit alterations in CC tract architectures, including 1 $DCC^{+/-}$/MM^{-} individual with partial agenesis of the CC. Thus, whereas decreased lateralization of the CST and movement-induced motor representations depend upon the presence of MM, callosal abnormalities depend upon the presence of the $DCC^{+/-}$ mutation. Similarly, Marsh et al[8] observed independent expression of MM and callosal agenesis among $DCC^{+/-}$ individuals. These differential effects of the *DCC* mutation might reflect individual differences in the regionally specific expression of DCC; for example, suppression of DCC within CST neurons is not sufficient to disrupt CST crossing but selective inhibition of DCC within commissural neurons is sufficient to disrupt callosal decussation.[10] More generally, phenotypic differences between the 2 $DCC^{+/-}$ groups may be explained by more extensive and pervasive brain regional decreases in *DCC* expression, as suggested by the observation here that *DCC* mRNA reduction was associated with MM but not the $DCC^{+/-}$ mutation. Together, by identifying distinct phenotypes among *DCC* mutation carriers with and without MM, these findings affirm the critical role that DCC plays in the organization and function of commissural and CST fibers in humans.

Acknowledgment

This work was supported by funding from the Canadian Institutes for Health Research (MOP-258547) and the National Institute on Drug Abuse (R01DA037911).

We thank Dr J. Correa, director of the McGill University Statistical Counselling Service, and I. Pokhvisneva for their guidance on the statistical analyses; Dr P. Pelufo Silveira for her feedback on the statistical design; and Drs J. Germann and J. Armony for providing advice and instructions on the fMRI analyses.

Author Contributions

Conception and design of the study: A.D., C.B., M.S., R.J., F.L., G.R., A.P.-L., M.F., C.F., M.L., H.T. Acquisition and analysis of data: D.E.V., V.B., A.T.-B., D.C., A.C., N.J., S.M.L.C., K.L., D.A., F.D., Y.Z., D.T., R.L.P. Drafting a significant portion of the manuscript or figures: D.E.V., V.B., A.T.-B., C.F., M.L., H.T.

Potential Conflicts of Interest

Nothing to report.

References

1. Finger JH, Bronson RT, Harris B, et al. The netrin 1 receptors Unc5h3 and Dcc are necessary at multiple choice points for the guidance of corticospinal tract axons. J Neurosci 2002;22:10346–10356.
2. Srour M, Rivière J-B, Pham JM, et al. Mutations in DCC cause congenital mirror movements. Science 2010;328:592.
3. Mayston MJ, Harrison LM, Stephens JA. A neurophysiological study of mirror movements in adults and children. Ann Neurol 1999;45: 583–594.
4. Capaday C, Forget R, Fraser R, Lamarre Y. Evidence for a contribution of the motor cortex to the long-latency stretch reflex of the human thumb. J Physiol 1991;440:243–255.
5. Cincotta M, Borgheresi A, Boffi P, et al. Bilateral motor cortex output with intended unimanual contraction in congenital mirror movements. Neurology 2002;58:1290–1293.
6. Cohen L, Meer J, Tarkka I, et al. Congenital mirror movements: abnormal organization of motor pathways in two patients. Brain 1991;114(pt 1B):381–403.
7. Gallea C, Popa T, Hubsch C, et al. RAD51 deficiency disrupts the corticospinal lateralization of motor control. Brain 2013;136: 3333–3346.
8. Marsh AP, Heron D, Edwards TJ, et al. Mutations in DCC cause isolated agenesis of the corpus callosum with incomplete penetrance. Nat Genet 2017;49:511–514.
9. Jamuar SS, Schmitz-Abe K, D'Gama AM, et al. Biallelic mutations in human DCC cause developmental split-brain syndrome. Nat Genet 2017;49:606–612.
10. Welniarz Q, Morel M-P, Pourchet O, et al. Non cell-autonomous role of DCC in the guidance of the corticospinal tract at the midline. Sci Rep 2017;7:410.
11. Ferbert A, Priori A, Rothwell J, et al. Interhemispheric inhibition of the human motor cortex. J Physiol 1992;453:525–546.
12. Fox MD, Snyder AZ, Vincent JL, et al. The human brain is intrinsically organized into dynamic, anticorrelated functional networks. Proc Natl Acad Sci U S A 2005;102:9673–9678.
13. Van Dijk KR, Hedden T, Venkataraman A, et al. Intrinsic functional connectivity as a tool for human connectomics: theory, properties, and optimization. J Neurophysiol 2010;103:297–321.
14. Fox MD, Greicius M. Clinical applications of resting state functional connectivity. Front Syst Neurosci 2010;4:19.
15. Buckner RL, Krienen FM, Castellanos A, et al. The organization of the human cerebellum estimated by intrinsic functional connectivity. J Neurophysiol 2011;106:2322–2345.
16. Yousry T, Schmid U, Alkadhi H, et al. Localization of the motor hand area to a knob on the precentral gyrus. Brain 1997;120(pt 1):141–157.
17. Coupé P, Yger P, Prima S, et al. An optimized blockwise nonlocal means denoising filter for 3-D magnetic resonance images. IEEE Trans Med Imaging 2008;27:425–441.
18. Garyfallidis E, Brett M, Amirbekian B, et al. Dipy, a library for the analysis of diffusion MRI data. Front Neuroinform 2014;8;8.
19. Tustison NJ, Avants BB, Cook PA, et al. N4ITK: improved N3 bias correction. IEEE Trans Med Imaging 2010;29:1310–1320.
20. Jenkinson M, Beckmann CF, Behrens TE, et al. FSL. Neuroimage 2012;62:782–790.
21. Smith SM. Fast robust automated brain extraction. Hum Brain Mapp 2002;17:143–155.
22. Andersson JL, Sotiropoulos SN. An integrated approach to correction for off-resonance effects and subject movement in diffusion MR imaging. Neuroimage 2016;125:1063–1078.
23. Descoteaux M, Deriche R, Knosche TR, Anwander A. Deterministic and probabilistic tractography based on complex fibre orientation distributions. IEEE Trans Med Imaging 2009;28:269–286.
24. Garyfallidis E, Ocegueda O, Wassermann D, Descoteaux M. Robust and efficient linear registration of white-matter fascicles in the space of streamlines. Neuroimage 2015;117:124–140.
25. Garyfallidis E, Côté M-A, Hau J, et al. Recognition of bundles in healthy and severely diseased brains. Paper presented at: 23rd Annual Meeting of the International Society for Magnetic Resonance in Medicine; May 30–June 5, 2015; Toronto, Ontario, Canada.
26. Witelson SF. Hand and sex differences in the isthmus and genu of the human corpus callosum: a postmortem morphological study. Brain 1989;112:799–835.
27. Torres-Berrío A, Lopez JP, Bagot RC, et al. DCC confers susceptibility to depression-like behaviors in humans and mice and is regulated by miR-218. Biol Psychiatry 2017;81:306–315.
28. Anderson MA, Gusella JF. Use of cyclosporin A in establishing Epstein-Barr virus-transformed human lymphoblastoid cell lines. In Vitro 1984;20:856–858.
29. Hibar DP, Stein JL, Renteria ME, et al. Common genetic variants influence human subcortical brain structures. Nature 2015;520:224–229.
30. Hoops D, Flores C. Making dopamine connections in adolescence. Trends Neurosci 2017;40:709–719.
31. Flores C. Role of netrin-1 in the organization and function of the mesocorticolimbic dopamine system. J Psychiatry Neurosci 2011;36: 296–310.
32. Betzel RF, Byrge L, He Y, et al. Changes in structural and functional connectivity among resting-state networks across the human lifespan. Neuroimage 2014;102:345–357.
33. Kochunov P, Williamson DE, Lancaster J, et al. Fractional anisotropy of water diffusion in cerebral white matter across the lifespan. Neurobiol Aging 2012;33:9–20.
34. Bhandari A, Radhu N, Farzan F, et al. A meta-analysis of the effects of aging on motor cortex neurophysiology assessed by transcranial magnetic stimulation. Clin Neurophysiol 2016;127:2834–2845.

35. Goldsworthy MR, Vallence A-M, Hodyl NA, et al. Probing changes in corticospinal excitability following theta burst stimulation of the human primary motor cortex. Clin Neurophysiol 2016;127: 740–747.

36. Fazeli A, Dickinson SL, Hermiston ML, et al. Phenotype of mice lacking functional deleted in colorectal cancer (Dcc) gene. Nature 1997;386:796.

37. Keino-Masu K, Masu M, Hinck L, et al. Deleted in colorectal cancer (DCC) encodes a netrin receptor. Cell 1996;87:175–185.

38. Depienne C, Bouteiller D, Méneret A, et al. RAD51 haploinsufficiency causes congenital mirror movements in humans. Am J Hum Genet 2012;90:301–307.

39. Leinsinger GL, Heiss DT, Jassoy AG, et al. Persistent mirror movements: functional MR imaging of the hand motor cortex. Radiology 1997;203:545–552.

40. Franz EA, Chiaroni-Clarke R, Woodrow S, et al. Congenital mirror movements: phenotypes associated with DCC and RAD51 mutations. J Neurol Sci 2015;351:140–145.